NJC

Accepted Manuscript

This is an *Accepted Manuscript*, which has been through the Royal Society of Chemistry peer review process and has been accepted for publication.

Accepted Manuscripts are published online shortly after acceptance, before technical editing, formatting and proof reading. Using this free service, authors can make their results available to the community, in citable form, before we publish the edited article. We will replace this *Accepted Manuscript* with the edited and formatted *Advance Article* as soon as it is available.

You can find more information about *Accepted Manuscripts* in the Information for Authors.

Please note that technical editing may introduce minor changes to the text and/or graphics, which may alter content. The journal's standard Terms & Conditions and the Ethical guidelines still apply. In no event shall the Royal Society of Chemistry be held responsible for any errors or omissions in this *Accepted Manuscript* or any consequences arising from the use of any information it contains.

ROYAL SOCIETY OF CHEMISTRY

www.rsc.org/njc

Manuscript ID NJ-ART-08-2014-001370

Title: Synergistic effect between WO_3 and g-C_3N_4 towards efficient visible-light-driven photocatalytic performance

TOC

The first time fabricated morphology-based WO_3/g-C_3N_4 photocatalyst showed efficient enhanced photocatalytic performance for the degradation of Rhodamine B under visible light. The apparent activity was 3.65 and 3.72 times greater than pure WO_3 and g-C_3N_4 respectively.

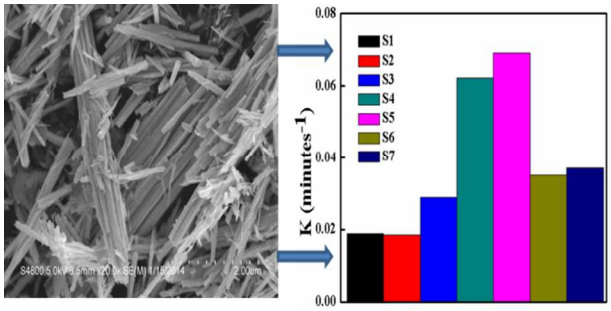

Cite this: DOI: 10.1039/c0xx00000x

www.rsc.org/xxxxxx

ARTICLE TYPE

Synergistic effect between WO_3 and g-C_3N_4 towards efficient visible-light-driven photocatalytic performance

Imran Aslam[a], Chuanbao Cao*[a], Muhammad Tanveer[a], Waheed Samraiz Khan[a], Muhammad Tahir[a], Muhammad Abid[b], Faryal Idrees[a], Faheem Khurshied Butt[a], Zulfiqar Ali[a] and Nasir Mahmood[c]

Received (in XXX, XXX) XthXXXXXXXXX 20XX, Accepted Xth XXXXXXXXX 20XX
DOI: 10.1039/b000000x

We have developed a facile, scaled up, efficient and morphology-based novel WO_3/g-C_3N_4 photocatalyst with different mass ratios of WO_3 and g-C_3N_4. It was used for the photodegradation of Rhodamine B (RhB) under visible light irradiation and it showed excellent enhanced photocatalytic efficiency as compared to pure g-C_3N_4 and WO_3. The apparent performance of the (composite/hybrid) was 3.65 times greater than pure WO_3 and 3.72 times than pure g-C_3N_4 respectively, and it was also found to be much higher than the previously reported ones. Further, the optical properties of composite samples were evaluated. The bandgap of composite samples lies in the range of 2.3-2.5 eV which was favourable for photodegradation. The possible mechanism for enhanced catalytic efficiency of the WO_3/g-C_3N_4 photocatalyst is discussed in detail. It was found that the enhanced performance is due to synergistic effect between WO_3 and g-C_3N_4 interface, improved optical absorption in visible region and suitable band positions of WO_3/g-C_3N_4 composites.

Introduction

The fabrication of semiconductor photocatalysts with high performance for pollutant degradation has become an attractive topic for researchers nowadays. The visible-light-driven photocatalysts have received a great attention in this regard [1–3]. After the report of Fujishima and Honda [4], TiO_2 became the most widely used semiconductor photocatalyst [5, 6] due to its low price, non-toxicity and good performance. However, low solar energy conversion efficiency due to wide band gap (3.2 eV) and high recombination rate of photogenerated electron–hole pairs have hampered its industrial applications [7, 8]. Therefore, efforts are still being carried out to synthesize novel photocatalysts that have strong visible light response and high catalytic efficiency as well.

Tungsten trioxide (WO_3), a transition metal oxide semiconductor with a band gap 2.6-2.8 eV, has been introduced as an alternative photocatalyst with a lot of potential applications such as visible-light-driven photocatalysts and related technological applications [9-13]. However, it has been observed that under visible light it shows a limited catalytic activity because its conduction band edge lies in a position not favourable for single-electron reduction of O_2 which makes it a less efficient photocatalyst for organic degradation [14]. On the other hand, graphite-like carbon nitride (g-C_3N_4) [15-17] a metal free and nontoxic material has emerged as one of the promising candidates for photocatalysis especially after the report of Wang *et al.* [18]. Although g-C_3N_4 has shown a great potential for catalytic activities but small surface area and high recombination rate of photogenerated electron-hole pairs are the factors that limit its performance [19, 20]. Two-dimensional (2D) nanostructures, the analogous to graphene have acquired remarkable interest due to their extraordinary optoelectronic and mechanical properties. The unique feature of 2D anisotropy helps to gain new physiochemical properties. It is reported that g-C_3N_4 nanosheets can have an electronic band structure with band edges straddling the water redox potentials making them a promising catalyst for water-splitting to produce hydrogen under sunlight [21, 22]. g-C_3N_4 is a soft polymer, can easily be coated on the surface of others compounds which may help for the transport of photogenerated charge carriers and hence can be used as an efficient co-catalyst for semiconductor-based photocatalysts to improve their catalytic activity [23]. One-dimensional (1D) single crystalline structures are of great importance, as they have a potential ability to provide direct path to photogenerated charges, with reduced grain boundaries and results in superior charge transport properties [24-26]. Further, 1D nanostructures can provide high surface to volume ratio with less defects. Recently, the coupling of two kinds of photocatalysts with small band gap has become a novel technique to overcome the problems of traditional photocatalysts [27, 28]. Hybrid/heterostructured materials are considered to be good candidates for photon-to-fuel conversion. They provide excellent charge separation and slow down recombination and high separation of photo-induced electron-hole pairs at the interface between two semiconductors which eventually causes the enhanced catalytic activity [29-32]. A lot of efforts including size-controlling [33, 34], noble-metal-loading [35, 36], coupling with other semiconductors have been devoted to enhance the photocatalytic activity of WO_3 [14, 37-40]. Among these studies, it has been confirmed that WO_3 is a good candidate for fabricating semiconductor heterojunctions to achieve higher catalytic efficiency. For example, the semiconductors Fe_2O_3 [14], TiO_2 [37], CuO [38], $CuBi_2O_4$ [39], and $CaFe_2O_4$ [40] *etc.,* have been coupled with WO_3 to make the heterostructured/hybrid photocatalysts and they exhibited

catalytic performance under visible light. It has been reported that synthesizing the heterostructures by mixing C_3N_4 with other semiconductors facilitates an easy path to promote the separation of photo-induced charge carriers and provides enhanced activity [41, 42]. So, keeping in mind the importance of 1D nanostructures and the problems regarding the traditional photocatalysts, we came up with an idea of synergetic approach to form a such hybrid system. There are only a few reports [43-45] on WO_3/C_3N_4 composites but not with some specific morphological structure. In these reports, they used powder or irregular shaped materials to make the composite and compared the performance of the prepared composite with powdered/irregular structured WO_3 and g-C_3N_4. We fabricated 1D WO_3 microrods and mixed them with 2D g-C_3N_4 sheets to gain the advantage of such geometry. This morphological-based synergism of 1D WO_3 microrods and 2D g-C_3N_4 sheets may increase the specific surface area and decrease the number of defects. As a result, the enhanced degradation activities were attained. Moreover, in the synergism of WO_3/g-C_3N_4, the former component helps to reduce the recombination rate of electron-hole pairs while the later one enhances the active sites of the catalyst surface [43, 44].

Herein, we have presented for the first time morphology-based novel WO_3/g-C_3N_4 (1D/2D) synergetic hybrid system fabricated by a simple hydrothermal and annealing method which exhibited superior photocatalytic activity and stability for the degradation of RhB under visible light irradiation. It can be found that after mixing g-C_3N_4 with WO_3, the catalytic efficiency and photo stability of the WO_3 microrods were substantially improved. The performance (rate constant 0.06912 min^{-1} or 4.1472 h^{-1}) of the present composite WO_3/g-C_3N_4 was much higher than that of the reported value [43]. The work provides new possibilities for hybrid geometries of nanostructures to enhance their properties by synergistic effect. Further, it may provide new insights for the practical application of WO_3 in hydrogen production. In the end, possible mechanism for the enhanced activity of WO_3/g-C_3N_4 composite on the behalf of experimental results is discussed in detail.

Experimental Section

Fabrication of WO_3/g-C_3N_4

WO_3 microrods were prepared by hydrothermal treatment, initially 1.0314 g of $NaWO_4.2H_2O$ and 0.3714 g of NaCl were dissolved in 2 mL of 2 M HCl solution and stirred for 30 minutes, during the stirring add 23 mL distilled water and a light sky blue solution was transferred to autoclave and heated it at 180 ˚C for 48 hours. The obtained material was washed three times with distilled water and absolute ethanol respectively. The g-C_3N_4 powder was prepared according to literature [46]. Typically, 5.0 g of melamine were taken into an alumina crucible. The crucible was covered and heated at 550 ˚C in a muffle furnace with a rate of 2 ˚C min^{-1} for 4 hours.

The WO_3/g-C_3N_4 composite was synthesized as follows: the specific amounts of g-C_3N_4 and WO_3 were dispersed in 10 mL of ethanol separately in beakers and sonificated for 1 hour to obtain well dispersed homogeneous suspension. The g-C_3N_4 solution was then poured into the WO_3 solution and magnetically stirred it for 1 hour. The obtained solution was dried at 80 ˚C for 12 hours and then annealed at 350 ˚C for 4 hours with a rate of 5 ˚C/minutes. According to this method, we prepared the following samples with different mass ratios of WO_3/g-C_3N_4; 1:0 (S1), 0:1 (S2), 1:0.2 (S3), 1:0.5 (S4), 0.2:1 (S5), 0.5:1 (S6) and 1:1 (S7).

Characterization

The as-synthesized WO_3/g-C_3N_4 composite phase characterization was done by X-ray diffraction (XRD; Philips X'Pert Pro MPD), using a Cu Kα radiation source (λ = 0.15418 nm) with 2θ from 10˚ to 80˚. The morphology and composition of the as-prepared sample were analyzed by field emission scanning electron microscopy (FESEM), transmission electron microscope (TEM, H-600-II, and Hitachi) and the chemical composition of the samples was determined by an energy dispersive X-ray (EDX) analysis (Hitachi S-3500). Fourier transform infrared (FTIR) spectra of samples were recorded using a Nicolet Avatar-370 spectrometer at room temperature. The UV-VIS-NIR (Hitachi-4100) spectrophotometer was used to measure the optical absorption spectra and energy band gap and room temperature photoluminescence (PL) spectra were measured with a Hitachi FL-4500 fluorescence spectrometer.

Photocatalytic test

The photocatalytic properties of the as-synthesized WO_3/g-C_3N_4 were evaluated by the degradation of RhB under visible light. A 500 W Xenon lamp was used as a visible light source. In order to study the concentration of RhB in solution, the UV-VIS-NIR (Hitachi U-4100) spectrophotometer was used. For photocatalytic test, 0.40 L of 0.01 M RhB was taken in a glass beaker and 0.05 g of the sample material was dissolved in this solution. Prior to irradiation, the solution were magnetically stirred in the dark for 30 minutes to obtain the saturated absorption of RhB onto the catalysts and then brought this solution to the visible light. At the irradiation time intervals of every 10 minutes, 3 mL of the suspension were collected and centrifuged to remove the photocatalyst particles every time before measuring the absorption spectra. The initial concentration (C_0) was the maximum absorption peak of the RhB which was recorded as 554 nm. Further detail about the RhB dye can be found in supporting information (ESI†).

Results and discussion

Phase characterization and morphology

In the present work, we first synthesized WO_3 and g-C_3N_4 separately by hydrothermal and annealing method and then developed a novel hybrid system/composite WO_3/g-C_3N_4 using a simple physical mixing and annealing method by choosing different mass ratios of g-C_3N_4 and WO_3. Fig. 1 (a) shows the XRD pattern of WO_3 (S1) microrods, well-defined peaks with specific intensities can be indexed to hexagonal phase of WO_3 (JCPDS Card No. 75-2187 with lattice constants a=b=7.2980 Å, c=3.8990 Å and α=β =90°, γ =120°) with the following distinctive peaks at 14.0°, 22.83°, 28.17° and 36.57°

corresponding to (100), (001), (200) and (201) planes respectively. Fig. 1 (b) shows the XRD pattern of g-C_3N_4 (S2), there is only one broad peak appearing at 27.1° corresponding to g-(002) planes. Fig. 1 (c) represents the XRD patterns for all the samples of WO_3/g-C_3N_4 composites (S3-S7) and the highest peak was observed at 28.06° for all samples, which means that after the introduction of g-C_3N_4 the main peak of WO_3 slightly changed from original position and appeared with decreased intensities. But surprisingly not any peak of g-C_3N_4 was observed in the WO_3/g-C_3N_4 composites at all, which may be due to very low intensity of g-C_3N_4 as compared to WO_3. Since the main peak of pure WO_3 is much intense than g-C_3N_4, so when it was mixed with g-C_3N_4 to make composite, the peak of pure g-C_3N_4 couldn't appear there. Secondly, there is an interesting reason about the absence of g-C_3N_4 peak in the composite samples. As the main peak of g-C_3N_4 centred at 27.1° lies between the two WO_3 peaks positioned at 26.8° and 28.17° corresponding to (101) and (200) planes respectively. So, it is simply impossible for g-C_3N_4 peak to appear in the composite samples within a very small *d*-spacing interval. However, the presence of g-C_3N_4 can be confirmed from Fig. 1 (d). It shows a close view of main peaks of all the samples (S3-S7), and one can clearly see that the main peak of WO_3 is gradually decreased with the increase of g-C_3N_4 content. As g-C_3N_4 has low crystalline nature, so the addition of g-C_3N_4 into WO_3 affects the crytallinity of the as-prepared composites and decreases their peak intensity.

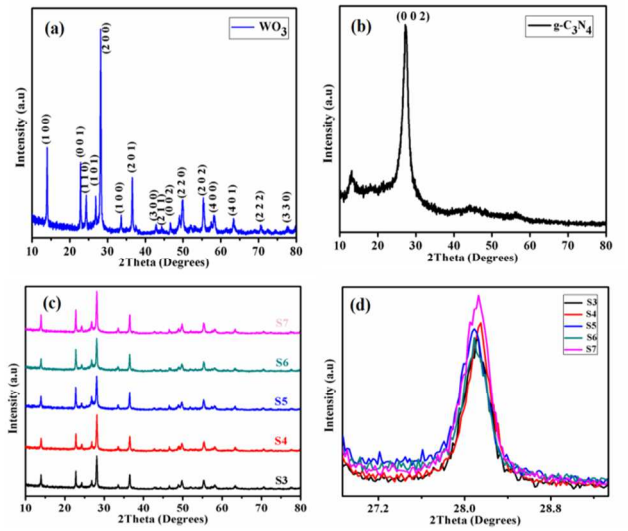

Figure 1 (a) XRD pattern of WO_3 (b) XRD pattern of g-C_3N_4 (c) XRD patterns of composite samples (S3-S7) (d) XRD patterns of composite samples in short range

Fig. 2 depicts the EDX spectrum of the composite WO_3/g-C_3N_4 (sample S5) while the inset of Fig. 2 shows elemental composition (wt %) contained by S5. It can be noticed that the as-synthesized composite is composed of only C, N, O and W elements which means that the as-prepared sample is pure and not any kind of impurity is present.

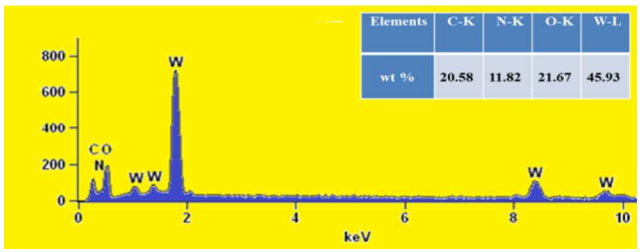

Figure 2 EDX spectrum of WO_3/g-C_3N_4 (S5)

The morphologies of the as-prepared materials are shown in Fig 3. Fig. 3 (a) shows the SEM image of pure WO_3 rods like structure. It can be observed from figure that the as-synthesized WO_3 rods are very dense and uniform. The diameter of these rods is in the range of 200-300 nm while the length in the range of 4-7 µm (Fig. S1 ESI†). Fig. 3 (b) shows the TEM image of sheets like structure of g-C_3N_4. It can be seen from figure that these sheets are arranged in layers. Fig. 3 (c-e) shows the FESEM images of the fabricated composite WO_3/g-C_3N_4 at different magnifications. The FESEM images in Fig. 3 (c-e) show the combination of rods and sheets like structure of WO_3/g-C_3N_4. In addition, we can see more clearly the rods and sheets like structure of WO_3/g-C_3N_4 (S5) from the TEM image in Fig. 3 (f).

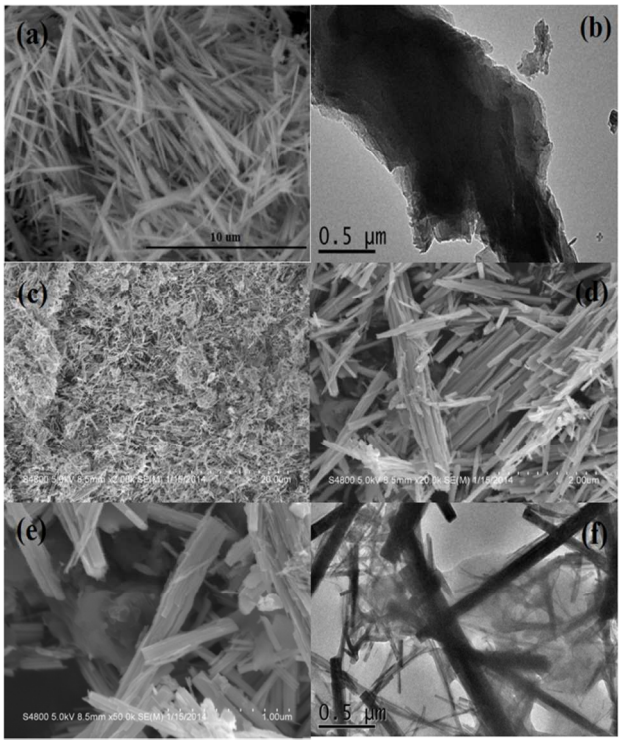

Figure 3 (a) SEM image of WO_3 rods, (b) TEM image of g-C_3N_4 sheets (c-e) FESEM images of the as-synthesized composite WO_3/g-C_3N_4 (sample S5) at different magnifications (f) TEM image of S5.

FTIR analysis

To further confirm the composition information and chemical bonding present in WO_3, g-C_3N_4 and WO_3/g-C_3N_4 composite samples, the FTIR spectra of all the samples were measured, as indicated in Fig. 4. Fig. 4 (a-c) shows the FTIR spectra of all the

samples, for WO_3 (S1), the absorption band around 820 cm^{-1} is clearly shown which corresponds to O–W–O stretching vibration in a monoclinic-type WO_3 crystal [47]. For g-C_3N_4 (S2), the FTIR confirms the presence of two main bonds in the products. The absorption peaks ranging from 800 to 1600 cm^{-1} are the strong indication of the heterocycles present in g-C_3N_4 [48, 49], these peaks are due to the breathing mode of s-triazine, sp^3 C–N bonds and sp^2 C=N. The peaks because of the stretching vibration modes of NH and NH_2 groups are observed in the range of 2500-3500 cm^{-1} in S2 [50, 51]. In the case of all other samples the intensity of peaks around 820 are not so high that may be due to presence of g-C_3N_4 [52] which can clearly be seen in Fig. 4 (b). The peaks observed in the range of 3000–3550 cm^{-1} may be attributed to the O–H stretching vibrations of physically absorbed water [53-55] and around 1380-1660 cm^{-1} could be correspond to H–O–H bending and O–H stretching vibrations of the adsorbed water molecules on the surface [56, 57].

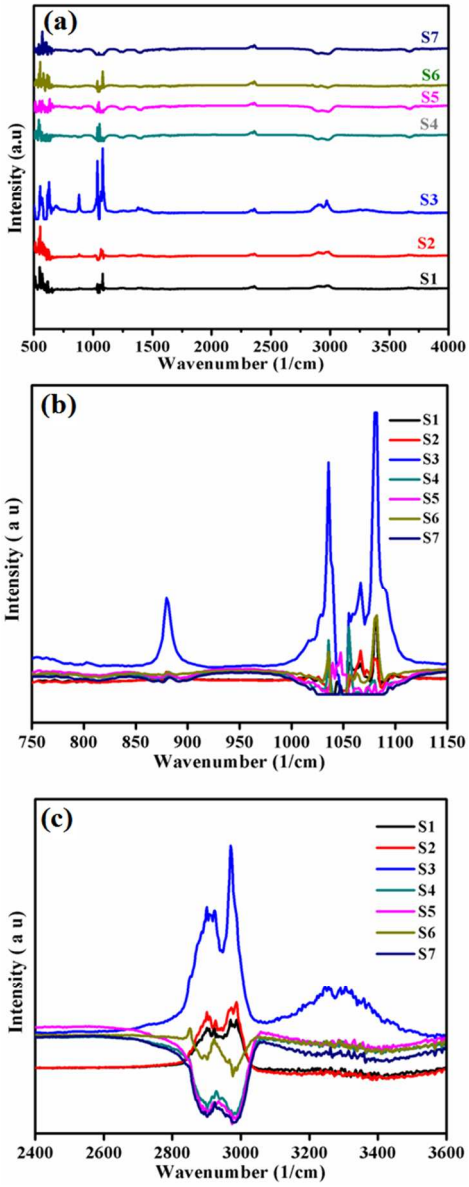

Figure 4 (a) FTIR of all the samples (b) FTIR of all the samples in short range (c) FTIR of all the samples in short range.

Optical absorption properties

Further, the UV spectra of WO_3, g-C_3N_4 and all the composite samples were examined, as can be seen in Fig. 5 (a-c). It can be noted that the absorption band edge for the case of pure WO_3 lies around 400 nm while for pure g-C_3N_4 around 410 nm as can be seen in Fig. 5 (c). The introduction of g-C_3N_4 into WO_3 causes the absorption edge shift towards the longer wavelength range and the absorption band edges for composite samples were recorded around 460 nm as shown in Fig. 5 (c). This shifting of absorption edges resulted in the decrement of band gaps. The decreased band gap of the composite samples can absorb more energy than pure samples which will excite more number of electrons from valence bands to conduction bands. As a result, more number of electron-hole pairs will be produced at the interface between two semiconductors and hence the catalytic performance will be improved. Fig. 5 (d) represents band gaps of all the samples as a function of g-C_3N_4 content. The graph is almost linear in the middle section from 0.16 to 0.66; we have thus controlled the band gap within the range 2.3-2.5 eV by suitable mass ratio of g-C_3N_4. Also it is strongly suggested that the band gap of composite of g-C_3N_4 with any other material can be reduced by following these mass ratios. It can be seen from figure that if we increase the concentration of g-C_3N_4 from a specific value, the band gap of the samples again started to increase which can be noticed from part of graph after 0.66 in Fig. 5 (d).

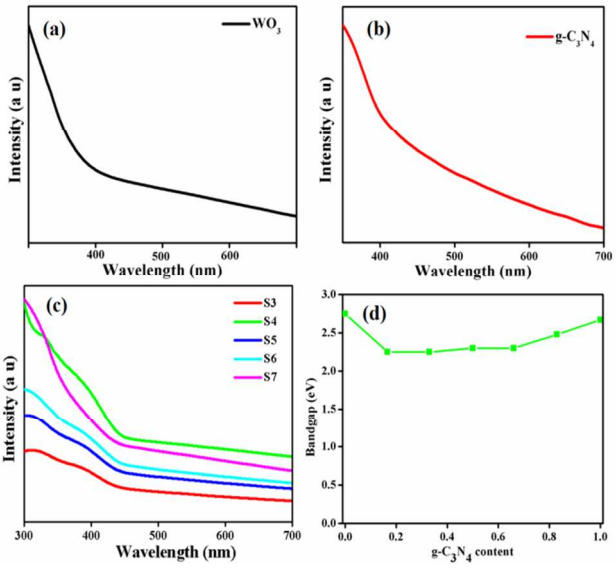

Figure 5 (a) UV spectrum of WO_3 (b) UV spectrum of g-C_3N_4 (c) UV spectra all the samples (S3-S7) (d) band gap of all the samples with respect to content ratio of g-C_3N_4.

The PL spectra of WO_3, g-C_3N_4 and all other samples were examined, as can be seen in Fig. 6 (a-c). The excitation wavelength for PL spectra was set at 300 nm. Both g-C_3N_4 and WO_3 separately have peaks around 460 nm which is due to their corresponding band gap. Fig. 6 (c) shows the PL of all other samples. It can be seen that when g-C_3N_4 sheets were added to WO_3 microrods, the emission intensity of the PL spectra for the WO_3/g-C_3N_4 composite was decreased which indicates that the

WO_3/g-C_3N_4 had a much lower recombination rate of photogenerated charge carriers. The intensity of S5 is minimum whereas S3 has maximum, which shows that S5 has less crystal defects than all other samples. These crystal defects acts as a recombination centre of hole and electron.

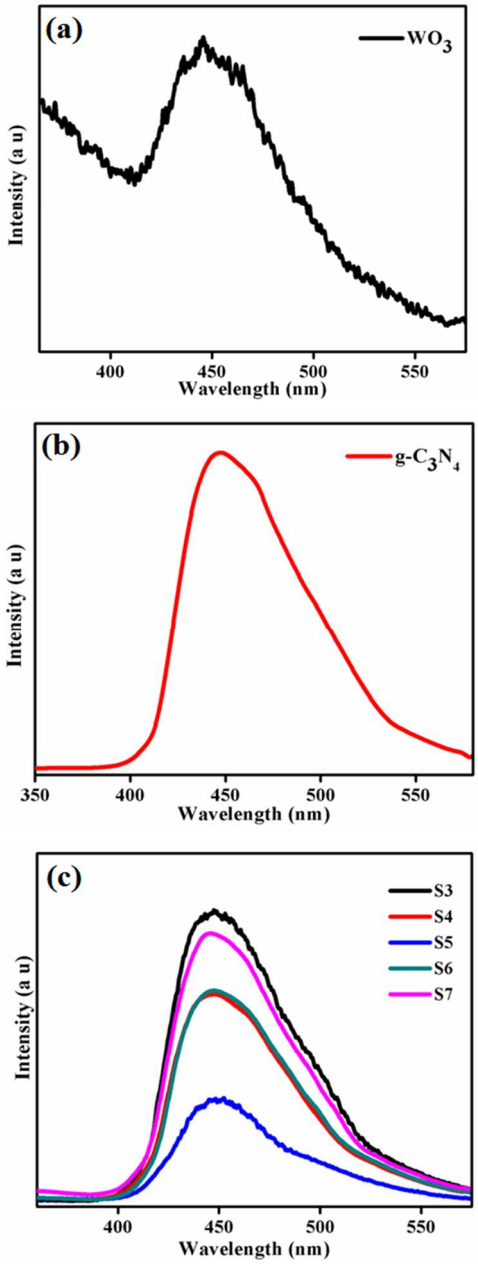

Figure 6 (a) PL spectrum of WO_3 (b) PL spectrum of g-C_3N_4 (c) PL spectra of all other samples.

Evaluation of photocatalytic activity

In order to investigate the photocatalytic property of the samples, photodegradation of RhB is performed. Fig. 7 (a) shows how the main peak of RhB is deceased with time. All the other samples are given in supporting information. Pure WO_3 takes 110 minutes while pure g-C_3N_4 takes 80 minutes to completely degrade RhB, whereas the sample S5 takes only 30 minutes for photodegradation of RhB as shown in Fig. 7 (a). The photodegradation of all other samples is given in Fig. S2 (ESI†).

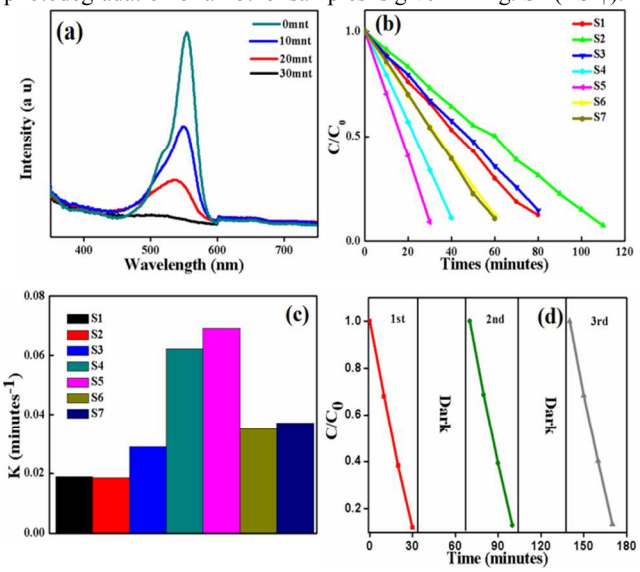

Figure 7 (a) Photodegradation of RhB with S5 (b) C/C_0 of all the samples (S1-S7) (c) *k* values of all the samples (S1-S7) (d) recyclability of S5.

Fig. 7 (b) shows the C/C_0 of all the samples and one sample is without any catalyst. It shows the first order rate constant *k* (min^{-1}) of WO_3 (S1), g-C_3N_4 (S2) and composite samples (S3-S7), which was calculated by the following first order equation:

$$\ln (C_0/C) = kt \quad (1)$$

where C_0 is the initial concentration of the dye in solution and C is the concentration of dye at time *t*. The sample without any catalyst shows no degradation at all the time which indicates that RhB is stable in water solution. Fig. 7 (c) shows the *k* vales of all the samples. It can be seen that the *k* value of S5 (0.06912 min^{-1}) is highest than that of all other samples. The reason is that the addition of g-C_3N_4 into WO_3 decreases the PL intensities of the composite samples as can be seen in Fig. 5 (c). The deceased PL intensities indicate slow recombination rate of photogenrated electron-hole pairs at the interface of composite samples which means that more number of electrons and holes take part in the oxidation and reduction reactions that results in the higher photocatalytic activity [58-60]. As for the case of S5, the PL intensity is lowest which means that the recombination rate of photogenrated charge carries for S5 is much slower than all other samples. Therefore, S5 shows the highest activity. The *k* values of pure WO_3 (0.01893 min^{-1}) and g-C_3N_4 (0.01856 min^{-1}) are almost equal as clear from Fig. 7 (c). When we increase the concentration of g-C_3N_4 in WO_3, the *k* value of the composites goes on increasing until the ratio of g-C_3N_4 and WO_3 reaches 0.2:1. After this stage, the *k* value of other samples is decreased which indicates that the ratio (0.2:1) for S5 was the best ratio for degrading RhB in visible light as cleared from Fig. 7 (c). Fig. 7 (d) shows the reusability of the S5, as for practical application it is also necessary that sample must be reusable and separate-able. After using three times, the efficiency of the material is not much affected as can be seen in Fig. 7 (d).

Proposed mechanism for enhanced photocatalytic performance of WO_3/g-C_3N_4

Fig. 7 shows the results of RhB degradation under visible light irradiation in the presence of the synthesized composite WO_3/g-C_3N_4 (S5). The excellent photodegradation of organic dye on the surface of WO_3/g-C_3N_4 composite under the visible light was occurred due to several factors. Firstly, there is a well-known factor that the heterostructured photocatalysts generally provide more reactive sites for catalysis and as well as for adsorption, so more organic pollutants are adsorbed that ultimately results in the fast photodegradation of the organic dye. Secondly, the very close contact of WO_3 rods and g-C_3N_4 sheets with each other in the synthesized composite facilitates the transfer of photogenerated electron hole pairs from one semiconductor to other. Because the single crystal structured WO_3 microrods provide a direct path for the transport of electrons to the composite surface unlike in a polycrystalline structure which is restricted by the grain boundaries. So, this easy transfer induces the high separation of the photogenerated charge carriers and enhances the photocatalytic reaction rate. Fig. 8 shows the energy band structure diagram of the fabricated WO_3/g-C_3N_4 composite/hybrid system. It can be noted from figure that the transfer of photogenerated electrons takes place from the conduction band (CB) of g-C_3N_4 to the CB of WO_3 and the photogenerated holes are transferred from the valence band (VB) of WO_3 to the VB of g-C_3N_4. When the composite samples were exposed to visible light source, electrons in the VB of WO_3 and g-C_3N_4 were excited to CB of WO_3 and g-C_3N_4 respectively. As a result, the holes were left in the VB of both materials, as can be seen in Fig. 8.

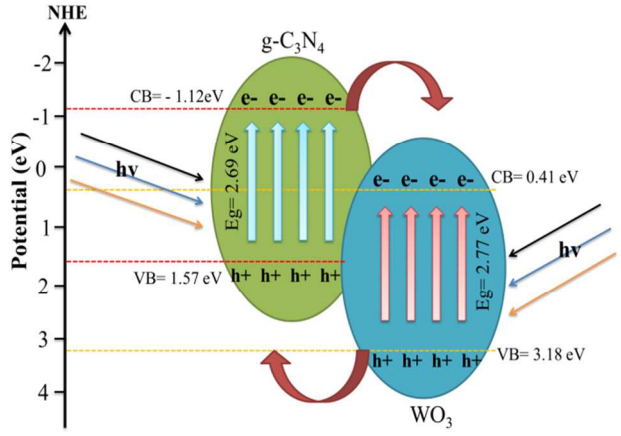

Figure 8 Schematic illustration of proposed mechanism for the photodegradation of RhB on WO_3/g-C_3N_4 composite

The valence and conduction band potentials of the pure g-C_3N_4 were found to be 1.57 eV and -1.12 eV [61], whereas for pure WO_3 their values were 3.18 eV and 0.41 eV respectively [62]. As the CB potential of g-C_3N_4 (−1.12 eV) is lower than that of WO_3 (0.41 eV), so the excited-state electrons from CB of g-C_3N_4 can directly transfer into the CB of WO_3. On the other hand, the VB potential of WO_3 (3.18 eV) is higher than that of g-C_3N_4 (1.57 eV), so the photogenerated holes from the VB of WO_3 can move to the VB of g-C_3N_4. The transfer of photo-induced electron hole pairs was accompanied by the consecutive reduction of W^{6+} into W^{5+} with the capture of photo-induced electrons at the trapping sites in WO_3 [63]. Simultaneously, the W^{5+} ions contained by WO_3 surface were re-oxidized into W^{6+} by the oxygen which was finally converted into O_2^-•. This movement results in the efficient separation of photogenerated electron-hole pairs and a slow-down recombination rate which consequently promotes the photonic efficiency for the degradation of organic pollutants. As hydroxyl radicals (•OH) are well known strong oxidants, that can contribute to the degradation process of RhB in the presence of water vapor in air. The molecules of water further reacting with photogenerated holes (h^+) or superoxide radicals (O_2^-•) at the photocatalyst surface can be converted to •OH by the following reactions [64];

$$h^+ + H_2O \rightarrow \bullet OH + H^+ \quad (2)$$

$$2O_2^-\bullet + 2H_2O \rightarrow 2\bullet OH + 2OH^- + O_2 \quad (3)$$

The photogenerated holes were captured by hydroxyl groups (OH^-) on the surface of photocatalyst and produced hydroxyl radicals •OH [65]. Similarly, hydrogen peroxide (H_2O_2) is also a strong oxidant, the oxygen molecules react with photo-excited electrons at the surface of WO_3 to be transformed into H_2O_2 through the following reaction [35];

$$O_2 + 2H^+ + 2e^- \rightarrow H_2O_2 \quad (4)$$

The as-produced superoxide anions (O_2^-•) either directly react with RhB or produce the hydroxyl radicals (•OH) by reacting with photo-induced electrons and hydrogen ions (H^+) [66, 67]. The strong oxidants, hydroxyl radicals (•OH), finally degraded the organic pollutant RhB. In addition, the excellent separation of photogenerated electron-hole pairs can be verified from the PL spectra of the photocatalyst. It can be noted from Fig. 5 (c) that the coupling of g-C_3N_4 with WO_3 microrods had an obvious effect on the PL intensities of the composite samples, the PL intensities were dramatically decreased which is strong evident of the slow recombination rate of photogenerated electron-hole pairs. As a result of this slow recombination the charge separation increases at the interface between two semiconductors, and the catalytic activity of WO_3/g-C_3N_4 composites thus enhanced was much higher than that of bare WO_3 and bare g-C_3N_4. The efficient separation of the charge carriers induced by hybrid effect, the low energy optical absorption under visible light and enhanced adsorption were some of the factors for significant enhancement in the photocatalytic activity. However, it has been noted that the separation of photo-induced electron-hole pairs depends on the suitable band-edge positions of the two semiconductors, because the band structure of the photocatalyst plays an important role in the separation process of the electron–hole pairs [68, 69]. The suitable band structure alignment of such semiconductors is favourable for charge accumulation/depletion at the interfaces which induces the separation of photo-induced electrons and holes [70] and as a result their photocatalytic efficiency is enhanced. We anticipate that the fabricated composite may also be useful for the hydrogen production via water splitting due to its favourable band gap, less recombination rate of electron-hole pairs and less number of crystal defects.

Conclusions

We have successfully prepared a novel WO_3/g-C_3N_4 visible-light-driven photocatalyst and used it for the photodegradation of Rhodamine B. The sample S5 of the as-prepared WO_3/g-C_3N_4 photocatalyst showed the highest photocatalytic efficiency. It has been noted that the as-synthesized WO_3/g-C_3N_4 composite (S5) exhibited performance 3.6 and 3.7 times as high as those of bare WO_3 and g-C_3N_4 under visible light irradiation respectively. The enhancement in the photocatalytic activity occurs by coupling g-C_3N_4 with WO_3 and is mainly due to following factors: (i) the synergistic effect between WO_3 and g-C_3N_4 (ii) high separation and easy transfer of photo-induced electron-hole pairs at the interface of composite, and (iii) the lower number of defects. The composite (WO_3/g-C_3N_4) can be easily synthesized by a simple physical mixing and annealing method and it can exhibit efficient photocatalytic performance under a variety of environments, particularly under visible (fluorescent) light. Moreover, it can be a good reference to develop more superior photocatalysts with high potential of using cheap solar light to utilize the energy and environmental problems.

Acknowledgements

This work was supported by National Natural Science Foundation of China (23171023，50972017) and the Research Fund for the Doctoral Program of Higher Education of China (20101101110026).

Notes and references

[a]Research Center of Materials Science, Beijing Institute of Technology, Beijing 100081, P. R. China
Email: cbcao@bit.edu.cn;
[b]School of Physics, Beijing Institute of Technology, Beijing 100081, P. R. China
[c]Department of Materials Science and Engineering, College of EngineeringPeking University, Beijing 100871, P. R. China

Electronic Supplementary Information (ESI) available: [Introduction of RhB, SEM images with lenth and diameter measurements, and photodegradation curves of WO_3/g-C_3N_4 (samples S1, S2, S3, S4, S6 and S7) can be seen in the supporting information].

[1] M. R. Hoffmann, S. T. Martin, W. Choi and D. W. Bahnemann, *Chem. Rev.,* 1995, **95**,69.
[2] (a) H. Choi, A. C. Sofranko and D. D. Dionysiou, *Adv. Funct. Mater.,* 2006, **16**, 1067; (b) M. Tanveer, Chuanbao Cao, Imran Aslam, Zulfiqar Ali, Faryal Idrees, Waheed S. Khan, Faheem K. Butt, Muhammad Tahir and Asif Mahmood, *Sci. Adv. Mater.,* 2014, doi:10.1166/sam.2014.1988.
[3] (a) Faryal Idrees, Chuanbao Cao, Faheem K. Butt, Muhammad Tahir, M. Tanveer, Imran Aslam, Zulfiqar Ali, Tariq Mahmood and Jianhua Hou, *CrystEngComm.,* 2013, **15**, 8146; (b) Faryal Idrees, Chuanbao Cao, R. Ahmed, Faheem K. Butt, Sajid Butt, Muhammad Tahir, Muhammad Tanvir, Imran Aslam, and Zulfiqar Ali, *Sci. Adv. Mater.,* 2014, doi:10.1166/sam.2014.2044.
[4] A. Fujishima and K. Honda, *Nature,* 1972, **238**, 37.
[5] (a) Shan Zheng, Wenjun Jiang, Yong Cai, Dionysios D. Dionysiou and Kevin E. O'Sheab, *Catalysis Today*, 2014, **224**, 88; (b) Faheem K. Butt, Muhammad Tahir, Chuanbao Cao, Faryal Idrees, R. Ahmed, Waheed Samraiz Khan, Zulfiqar Ali, Nasir Mahmood, Muhammad Tanveer, Asif Mahmood, and Imran Aslam, *ACS Appl. Mater. Interfaces*, 2014, DOI: 10.1021/am503136h.
[6] Wenjun Jiang, Jeffrey A. Joens, Dionysios D. Dionysiou and Kevin E. O'Shea, *J. Photochem. Photobiol. A: Chem.,* 2013, **262**, 13.
[7] (a) A. L. Linsebigler, G. Lu and J. T. Yates, *Chem. Rev.,* 1995, **95**, 735; (b) M. Tanveer, Chuanbao Cao, Zulfiqar Ali, Imran Aslam, Faryal Idrees, Waheed S. Khan, Faheem K. But, Muhammad Tahir and Nasir Mahmood, *CrystEngComm*, 2014, **16**, 5290.
[8] X. Chen and S. S. Mao, *Chem. Rev.*, 2007, **10**, 2891.
[9] Z. G. Zhao and M. Miyauchi, *Angew. Chem. Int. Ed.*, 2008, **47**, 7051.
[10] R. Liu, Y. Yin, L. Y. Chou, S. W. Sheehan, W. He, F. Zhang,H. J. Hou and D. Wang, *Angew. Chem. Int. Ed.,* 2011, **50**, 499.
[11] S. Wang, X. Feng, J. Yao and L. Jiang, *Angew. Chem. Int. Ed.,* 2006, **45**, 1264.
[12] Bing Zhang, Chuanbao Cao, Hailin Qiu, Yajie Xu, Yingchun Wang and Hesun Zhu, *Chemistry Letters,* 2005, **34**, 154.
[13] (a) Imran Aslam, Chuanbao Cao, Waheed S. Khan, Muhammad Tanveer, M. Abid, Faryal Idrees, Rabia Riasat, Muhammad Tahir, Faheem K. Butt and Zulfiqar Ali, *RSC Adv.,* 2014, **4**, 37914; (b) Kang Mingyang, Cao Chuanbao, Xu Xingyan and Liao Bo, *Chinese Science Bulletin,* 2008, **53**, 335.
[14] D. Bi and Y. Xu, *Langmuir,* 2011, **27**, 9359.
[15] Li Chao, Cao Chuanbao and Zhu Hesun, *Chinese Science Bulletin,* 2003, **48**, 1737.
[16] Jie Li, Chuanbao Cao, and Hesun Zhu, *Nanotechnology*, 2007, **18**, 115605.
[17] Fulin Huang, Chuanbao Cao, Xu Xiang, Ruitao Lv and Hesun Zhu, *Diamond and Related Materials,* 2004, **13**, 1757.
[18] X. Wang, K. Maeda, X. Chen, K. Takanabe, K. Domen, Y. Hou, X. Fu and M. Antonietti, *J. Am. Chem. Soc.,* 2009, **131**, 1680.
[19] (a) Muhammad Tahir, Chuanbao Cao, Faheem K. Butt, Faryal Idrees, Nasir Mahmood, Zulfiqar Ali, Imran Aslam, M. Tanveer, Muhammad Rizwan and Tariq Mahmood, *J. Mater. Chem. A,* 2013, **1**, 13949; (b) Muhammad Tahir, Chuanbao Cao, Faheem K. Butt, Sajid Butt,Faryal Idrees, Zulfiqar Ali, Imran Aslam, M. Tanveer, Asif Mahmood and Nasir Mahmood, *CrystEngComm,* 2014, **16**, 1825.
[20] (a) J. D. Hong, X. Y. Xia, Y. S. Wang and R. Xu, *J. Mater. Chem.,* 2012, **22**, 15006; (b) Muhammad Tahir, Chuanbao Cao,,Nasir Mahmood, Faheem K. Butt, Asif Mahmood, Faryal Idrees, Sajad Hussain, M. Tanveer, Zulfiqar Ali, Imran Aslam, *ACS Appl. Mater. Interfaces,* 2014, **6**, 1258.
[21] Shubin Yang, Yongji Gong, Jinshui Zhang, Liang Zhan, Lulu Ma, Zheyu Fang, Robert Vajtai , Xinchen Wang, and Pulickel M. Ajayan, *Adv. Mater.,* 2013, **25**, 2452.
[22] P. Niu, L. L. Zhang, G. Liu and H. M. Cheng, *Adv. Funct. Mater.*, 2012, **22**, 4763.
[23] Liying Huang, Hui Xu, Rongxian Zhang, Xiaonong Cheng, Jiexiang Xia, Yuangguo Xu and Huaming Li, *Appl. Surf. Sci.,* 2013, **283**, 25.
[24] M. Law, L. E. Greene, J. C. Johnson, R. Saykally and P. D. Yang, *Nat. Mater.,* 2005, **4**, 455.
[25] F. Qian, G. M. Wang and Y. Li, *Nano Lett.,* 2010, **10**, 4686.

[26] G. M. Wang, X. Y. Yang, F. Qian, J. Z. Zhang and Y. Li, *Nano Lett.,* 2010, **10**, 1088.
[27] J. Cao, B. Xu, B. Luo, H. Lin and S. Chen, *Catal. Commun.,* 2011, **13**, 63.
[28] L. Zhang, K. H. Wonga, Z. Chen, J. C. Yu, J. Zhao, C. Hu, C. Y. Chan and P. K. Wong, *Appl. Catal. A: Gen.,* 2009, **363**, 221.
[29] J. Jiang, X. Zhang, P. B. Sun and L. Z. Zhang, J. Phys. Chem. C, 2011, 115, 20564.
[30] Y. Y. Wen, H. M. Ding and Y. K. Shan, *Nanoscale,* 2011, **3**, 4417.
[31] K. H. Reddy, S. Martha and K. M. Parida, *Inorg. Chem.,* 2013, **52**, 6401.
[32] J. J. Guo, S. X. Ouyang, P. Li, Y. J. Zhang, T. Kako and J. H. Ye, *Appl. Catal., B,* 2013, **134–135**, 292.
[33] W. Morales, M. Cason, O. Aina, N. R. de Tacconi and K. Rajeshwar, *J. Am. Chem. Soc.,* 2008, **130**, 6319.
[34] D. Hidayat, A. Purwanto, W. N. Wang and K. Okuyama, *Mater. Res. Bull.,* 2010, **45**, 173.
[35] R. Abe, H. Takami, N. Murakami and B. Ohtani, *J. Am. Chem. Soc.,* 2008, **130**, 7781.
[36] M. Qamar, M. A. Gondal and Z. H. Yamani, *Catal. Commun.,* 2010, **11**, 772.
[37] S. A. K. Leghari, S. Sajjad, F. Chen and J. Zhang, *Chem. Eng. J.,* 2011, **166**, 915.
[38] H. Widiyandari, A. Purwanto, R. Balgis, T. Ogi and K. Okuyama, *Chem. Eng. J.,* 2012, **180**, 329.
[39] T. Arai, M. Yanagida, Y. Konishi, Y. Iwasaki, H. Sugihara and K. Sayama, *J. Phys. Chem. C,* 2007, **111**, 7577.
[40] Z. F. Liu, Z. G. Zhao and M. Miyauchi, *J. Phys. Chem. C,* 2009, **113**, 17132–17137.
[41] S. Yan, S. Lv, Z. Li and Z. Zou, *Dalton Trans.,* 2010, **39**, 1488.
[42] C. Pan, J. Xu, Y. Wang, D. Li and Y. Zhu, *Adv. Funct. Mater.,* 2012, **22**, 1518.
[43] Liying Huang, Hui Xu, Yeping Li, Huaming Li, Xiaonong Cheng, Jixiang Xia, Yuanguo Xua and Guobin Cai, *Dalton Trans.,* 2013, **42**, 8606.
[44] Yipeng Zang, Liping Li, Ying Zuo, Haifeng Lin, Guangshe Li and Xiangfeng Gua, *RSC Advances,* 2013, **3**, 13646.
[45] Ken-ichi Katsumata, Ryosuke Motoyoshi, Nobuhiro Matsushita, Kiyoshi Okada, *J. Hazard. Mater.,* 2013, **260**, 475.
[46] Y. Wang, R. Shi, J. Lin and Y. Zhu, *Energy. Environ. Sci.,* 2011, **4**, 2922.
[47] C. Guéry, C. Choquet, F. Dujeancourt, J. M. Tarascon and J. C. Lassègues, *J. Solid State Electrochem.,* 1997, **1**, 199.
[48] V.N. Khabashesku, J.L. Zimmerman and J.L. Margrave, *Chem. Mater.,* 2000,**12**, 3264.
[49] X. Li, J. Zhang, L. Shen, Y. Ma, W. Lei, Q. Cui and G. Zou, *Appl. Phys. A*, 2009, **94**, 387.
[50] S.C. Yan, Z.S. Li and Z.G. Zou, *Langmuir*, 2009, **25**, 10397.
[51] M. J. Bojdys, J.O. Müller, M. Antonietti, A. Thomas, *Chem. Eur. J.,* 2008, **14**, 8177.
[52] M. Yang, Q. Huang and X. Jin, *Mater. Sci. Eng. B,* 2012,**177**, 600.
[53] Yan, S. C.; Li, Z. S.; Zou, Z. G. *Langmuir* **2009**, *25*, 10397-10401.
[54] Fu, J.; Tian, Y. L.; Chang, B. B.; Xi, F. N.; Dong, X. P. *J. Mater. Chem.* **2012**, *22*, 21159-21166.
[55] Bojdys, M. J.; Muller, J. O.; Antonietti, M.; Thomas, A. *Chem. Eur. J.* **2008**, *14*, 8177-8182.
[56] Kumar, S.; Surendar, T.; Baruah, A.; Shanker, V. *J. Mater. Chem. A* **2013**, *1*, 5333-5340.
[57] H. I. S. Nogueira, A. M. V. Cavaleiro, J. Rocha, T. Trindade, J. D. P. D. Jesus, Mater. Res. Bull., 2004, **39**, 683.
[58] Y. Yang, G. Zhang, S. Yu and X. Shen, Chem.–Eng. J., 2010, 162, 171–177.
[59] S. F. Chen, W. Zhao, W. Liu, H. Y. Zhang and X. L. Yu, J. Hazard. Mater., 2009, 172, 1415–1423.
[60] H. Huang, D. Li, Q. Lin, W. Zhang, Y. Shao, Y. Chen, M. Sun and X. Fu, Environ. Sci. Technol., 2009, 43, 4164–4168.
[61] L. Ge, C. C. Han and J. Liu, *Appl. Catal., B,* 2011, **108**, 100.
[62] S. J. Hong, S. Lee, J. S. Jang and J. S. Lee, *Energy Environ. Sci.*, 2011, **4**, 1781.
[63] V. Keller, P. Bernhardt and F. Garin, *J. Catal.,* 2003, **215**, 129.
[64] G. Vincent, P.M. Marquaire and O. Zahraa, *J. Hazard. Mater.,* 2009, **161**, 1173.
[65] N. Zhang, S. Q. Liu, X. Z. Fu and Y. J. Xu, *J. Phys. Chem. C*, 2011, **115**, 9136.
[66] L. R. Zheng, Y. H. Zheng, C. Q. Chen, Y. Y. Zhan, X.Y. Lin, Q. Zheng, K. M. Wei and J. F. Zhu, *Inorg. Chem.,* 2009, **48**, 1819.
[67] O. Legrini, E. Oliveros and A. M. Braun,*Chem. Rev.,* 1993, **93**, 671.
[68] J. Tersoff, *Phys. Rev. B,* 1984, **30**, 4874.
[69] Z. Alferov, *Semiconductors,* 1998, **32**, 1.
[70] J. Zhang, M. Zhang, R. Q. Sun and X. Wang, *Angew. Chem. Int. Ed.,* 2012, **51**, 10145.